J Solid State Electrochem (2010) 14:931–936
DOI 10.1007/s10008-009-0885-3

ORIGINAL PAPER

One-pot template-free synthesis, formation mechanism, and lithium ions storage property of hollow SnO_2 microspheres

Lifen Xiao · Jianping Li · Qiao Li · Lizhi Zhang

Received: 16 March 2009 / Revised: 6 June 2009 / Accepted: 9 June 2009 / Published online: 27 June 2009

Abstract In this work, we report a facile one-pot template-free approach to prepare hollow rutile SnO_2 microspheres using $SnCl_4$ as the precursor in a condensed H_2SO_4–EtOH mixed solvent. The formation mechanism of the hollow microspheres was proposed on the basis of characterizations. First, the controlled hydrolysis and condensation of $SnCl_4$ to SnO_2 nanocrystals was realized by the formation of water via catalytic dehydration of EtOH in the presence of condensed H_2SO_4. These SnO_2 nanocrystals rapidly aggregated to form microspheres in order to minimize their surface energies. Then, Ostwald ripening mechanism governed the subsequent growth and recrystallization of the nanocrystals to form the hollow structure. The resulting hollow SnO_2 microspheres exhibited better cycle performance than the pristine SnO_2 nanoparticles when used as anode materials in lithium ion batteries.

Keywords Porous materials · Nanocrystalline materials · Ostwald ripening · Hollow SnO_2 · Lithium ion battery · Anode

Introduction

SnO_2 with an n-type wide-band gap (E_g=3.6 eV) is a functional material of great interest, which has been widely applied in gas sensors, catalyst supports, optical devices, and lithium ion batteries. It is also well documented that the performances of SnO_2 in these applications intimately depend on its morphological and structural features. Thus, great efforts have been devoted to develop novel synthetic routes to produce diversely structured SnO_2 such as nanotubes, nanorods, nanobelts, hollow spheres, and mesoporous structures [1–11]. Particularly, hollow structures have attracted considerable attention because of their improvable performance, such as large surface area, efficient catalytic activity, and structural stability [4, 7–9, 11].

Templating is an available technique to tailor the simple hollow nanostructures. Various removable templates such as polymer latex spheres, carbon spheres, micelles, and vesicles [12–15] could be used. However, to obtain pure hollow materials, these templating strategies need remove template through calcination at elevated temperatures or wet chemical etching with appropriate solvent. In some cases, the construction would be destroyed or the wall has poor mechanical strength during the template removal process. Recently, the utilization of some physical phenomena, such as the Kirkendall effect [16, 17], gas bubble nucleation [18], and Ostwald ripening [19–24], to fabricate hollow structures provide new alternative opportunities for the template-free fabrication of hollow structures. Among them, Ostwald ripening has been proven to be a more facile approach to generate hollow structure. A large variety of hollow materials, such as TiO_2, SnO_2, Fe_2O_3, CuO, Cu_2O, Co_3O_4, $LnPO_4$, and $CdMoO_4$, have been prepared via this method.

SnO_2 is considered as a potential anode material for lithium ion batteries. It has relatively higher lithium insertion potential and theoretical capacity (about 790 mAh g^{-1}), which make it more energy density attractive and safety reliable than the widely used graphite material. However, the practical application of SnO_2 is hampered by its drastic specific volume change (about 358%) during Li insertion/extraction processes, which leads

L. Xiao (✉) · J. Li · Q. Li · L. Zhang
Key Laboratory of Pesticide & Chemical Biology of Ministry of Education, College of Chemistry, Central China Normal University, Wuhan 430079, People's Republic of China
e-mail: lfxiao@mail.ccnu.edu.cn

to fast mechanical failure of the electrode so as to poor cyclability. In order to solve this problem, many researchers attempted to disperse the nanoparticulate SnO_2 into carbon matrix or synthesize SnO_2@C core/shell structured nanocomposites [25, 26]. The carbon can act as a buffering matrix to relax the expansion and also can act as a barrier to suppress the aggregation of SnO_2 particles into larger and inactive SnO_2 clusters and thus increase their structure stability during cycling. On the other hand, it has been verified that three dimensionally nanostructured SnO_2 electrodes can exhibit enhanced structural stability in repetitive charging and discharging of the battery. It is believed that the hollow structure with large surface areas and short diffusion pathways for facile lithium-ion transport and as a means to recapture the SnO_2 nanoparticles once they are detached from the internal surface, so they have much tolerance for the large specific volume change in repetitive Li insertion/extraction [4, 8, 11, 14]. Herein, we introduce a novel one-pot template-free method to synthesize hollow SnO_2 microspheres. The synthesis is performed in an H_2SO_4–EtOH mixed solvent using $SnCl_4$ as the precursor and combines the controlled hydrolysis and condensation of $SnCl_4$ and Ostwald ripening process together. We assembled the as-prepared SnO_2 hollow spheres as an active anode material in lithium-ion batteries and compare lithium ions storage property with that of pristine SnO_2 nanoparticles synthesized in the absence of condensed H_2SO_4.

Experimental procedure

Synthesis In a typical procedure, 0.351 g of $SnCl_4{\cdot}5H_2O$ was dissolved in 18 mL of anhydrous EtOH-condensed H_2SO_4 mixed solvent. The volume of H_2SO_4 was 0.6 mL. The resulting transparent solution was transferred into a Teflon cup of 22 ml inner volume, slid into a steel autoclave, and carefully sealed. After heated in a furnace at 180 °C for 24 h, the autoclave was cooled down naturally. The white precipitate was collected by centrifugation, thoroughly washed with deionized water, and finally dried at 60 °C in the air. Caution: As the reaction produced a large number of gases, the internal pressure of the autoclave would become very high, so the solution could rush out with the gas flow when opening the cover of the autoclave!

Characterization The X-ray diffraction (XRD) patterns of the products were recorded on a Rigaku D/MAX-RB diffractometer with Cu Ka radiation. Scanning electron microscope (SEM) images were performed on a JSM-5600 scanning electron microscope and transmission electron microscope (TEM) images were performed on a JEM-2010FEF transmission electron microscope. Infrared spectra were measured on the Fourier infrared spectrum instrument (Nicolet Magna-IR 750). The nitrogen adsorption and desorption isotherms at 77 K were measured using a Micrometrics ASAP2020 system after samples were vacuum-dried at 200 °C overnight. Gas chromatography–mass spectrometry (GC–MS) analysis was carried out on a FINNIGAN Trace DSQ II device. The final reaction solution consists of two liquid phases; only the upper organic phase was subject to GC–MS analysis. The liquids were directly injected into the GC device.

Eletrochemical tests The lithium storage performance was tested using a typical three-electrode construction. The composite electrodes were consisted of 85% SnO_2 powders, 7% acetylene black, and 8% poly(tetrafluoroethylene) by weight and prepared by roll pressing the mixture into an electrode film, then pressing the electrode film onto an nickel net. The reference and counter electrodes were lithium sheets. The electrolyte used in this study was 1 mol L^{-1} $LiPF_6$/ethylene carbonate–dimethyl carbonate–ethylene methyl carbonate (1:1:1, *v*/*v*/*v*). The charge–discharge measurements were carried out using a BTS-55 Newware Battery charger. The cyclic voltammetry (CV) was carried out with a CHI660A Electrochemical Workstation.

Results and discussion

Figure 1 shows the XRD pattern of the product prepared via solvothermal reaction at 180 °C for 24 h in 18 mL of anhydrous EtOH-condensed H_2SO_4 (0.6 mL) mixed solvent. The strong and sharp diffraction peaks indicate the good crystallization of the product. All the diffraction peaks can be

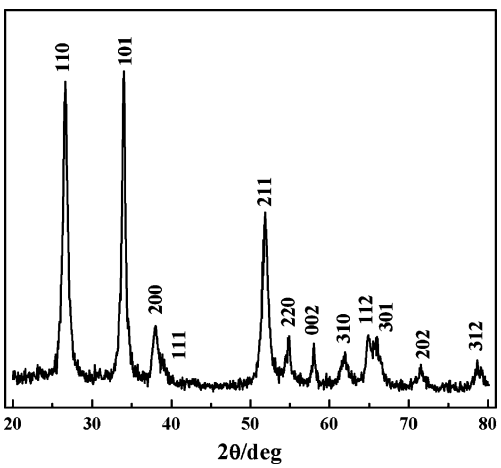

Fig. 1 XRD pattern of the hollow SnO_2 microspheres prepared at 180 °C for 24 h

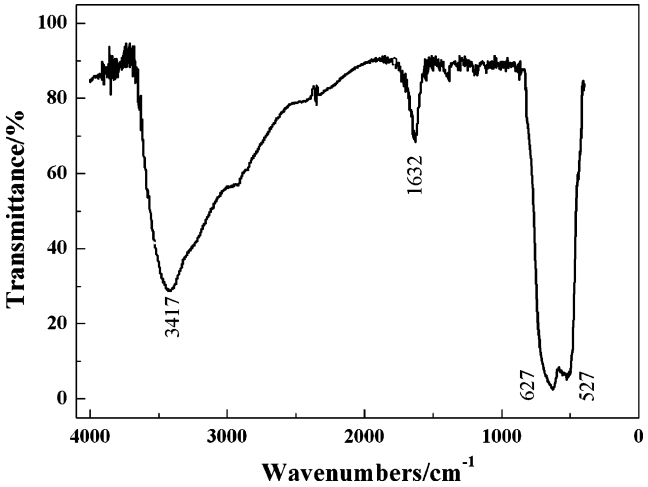

Fig. 2 FT-IR of the as-prepared hollow SnO_2 microspheres

perfectly indexed to a rutile structure of SnO_2 (JCPDS file No. 41-1445) with a=4.731 Å and c=3.182 Å. Only diffraction peaks belonging to SnO_2 are detected, implying the high purity of the final product. By using Scherer's formula, the mean crystalline size of the SnO_2 nanoparticles calculated from the FWHM of (110) peak is about 10.9 nm.

Figure 2 shows the infrared spectrum recorded for as-prepared SnO_2 hollow microspheres, which is consistent with that of the standard SnO_2. The wide peak at 3,417 cm^{-1} and weak peak at 1,632 cm^{-1} are typical of the O–H vibration due to the absorbed water. The bands at around 627 and 527 cm^{-1} can be attributed to the Sn–O stretching vibration and the O–Sn–O antisymmetric vibration in SnO_2.

Figure 3 shows the SEM and TEM images of hollow SnO_2 microspheres. The SEM image reveals that the product consists of plenty of microspheres with around 0.5–1 μm in size. The hollow interiors can be unambiguously observed from a number of microspheres with open mouths shown in the SEM image. Figure 3c shows a broken microsphere. The walls are about 200–300 nm in thickness and composed of very fine primary SnO_2 nanocrystals of about 10 nm, consistent with the calculated value according to the XRD data. The TEM image in Fig. 3d shows the lighter center and the darker edge of the spheres, confirming the hollow structure.

Figure 4 shows the N_2 adsorption–desorption isothermal plot of the as-synthesized hollow SnO_2 microspheres. The product displayed a type IV curve with a type H4 hysteresis loop in the range of 0.2–1.0 P/P_o, which is indicative of mesoporosity. The Barrett–Joyner–Halenda analysis shows that the Brunauer–Emmett–Teller surface area and pore size of the product are 51.4 $m^2\ g^{-1}$ and 5.6 nm, respectively. The mesopores are believed to be formed through the agglomeration of nanoparticles among the wall of the hollow SnO_2 microspheres, as revealed in Fig. 3c.

In order to understand the formation parameters of hollow SnO_2 microspheres, a series of comparison experiments under different H_2SO_4 contents, reaction durations,

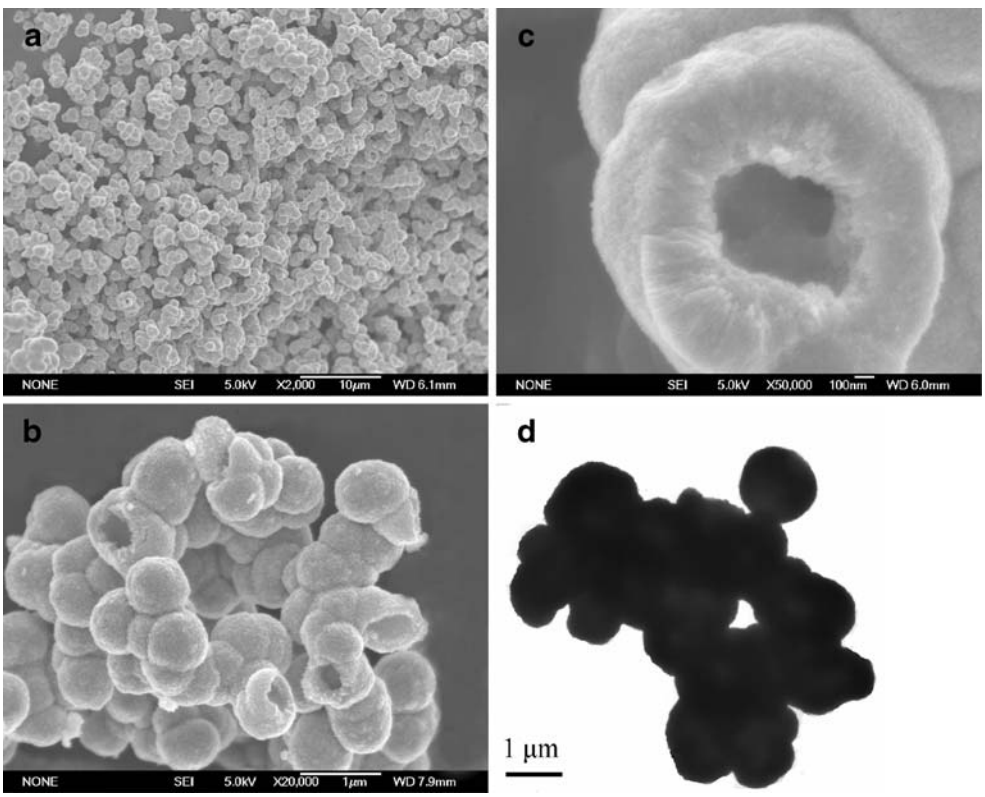

Fig. 3 Morphology of the as-prepared hollow SnO_2 microspheres. **a**, **b** SEM images of overall product. **c** Typical magnified SEM image of a hollow sphere. **d** TEM image of the product

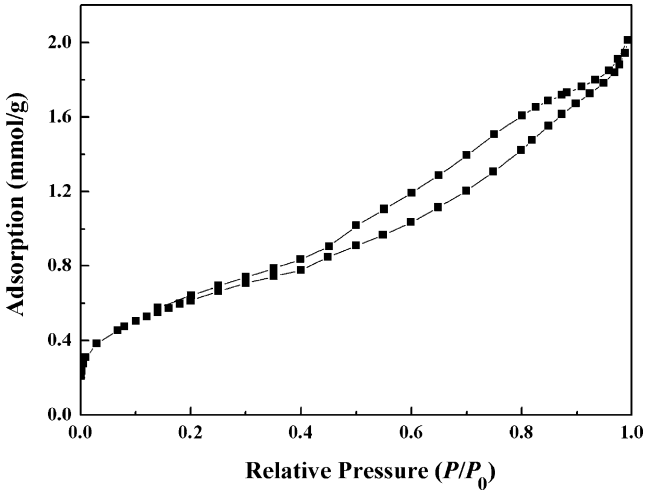

Fig. 4 N_2 adsorption–desorption isotherms of the hollow SnO_2 microspheres

and temperatures were carried out. It was found that the formation of hollow SnO_2 microspheres strictly depended on some experimental factors. First, the reaction temperatures strongly influence the formation of hollow spheres. Solid microspheres would form at lower temperatures of 140 °C. Although hollow spheres could be observed at 160 °C, the higher reaction temperature of 180 °C ensured the production of plenty of hollow microspheres in the as-prepared sample. Besides the temperature, the content of condensed H_2SO_4 in the EtOH also has a significant effect on the formation of hollow SnO_2 microspheres. The minimum volume of H_2SO_4 in 18 mL of total reaction solution was 0.3 mL H_2SO_4 for the formation of hollow microspheres. Only small nanoparticles were obtained when the volume of H_2SO_4 was less than 0.3 mL. However, excess H_2SO_4 would cause carbonization of the ethanol solvent. Therefore, 0.6 mL of H_2SO_4 and 180 °C was chosen finally.

After finding out the formation parameters of hollow SnO_2 microspheres, the time-dependent experiments were designed to record the morphologies of the products at different growth stages to understand the formation mechanism (Fig. 5). When the reaction time was as short as 3 h, only aggregated solid spheres were found in the product (Fig. 5a). After prolonging the reaction time to 6 h, hollow structure appeared as revealed by some broken spheres in Fig. 5b. Meanwhile, separated particles were also visible in this sample. Further extending the reaction time to 12 h, the thickness of the wall is noticeably decreased, accompanying the appearance of some core–shell structures (Fig. 5c). After 24 h, the core totally disappeared and complete hollow SnO_2 microspheres with high product yield and morphological yield were obtained (Fig. 5d).

It is known that under the catalysis of condensed H_2SO_4, EtOH could be dehydrated to give birth to water and organic compounds (ether and/or ethylene, etc). We found that the reacted solutions consisted of two liquid phases, an upper organic phase and a lower condensed H_2SO_4 phase.

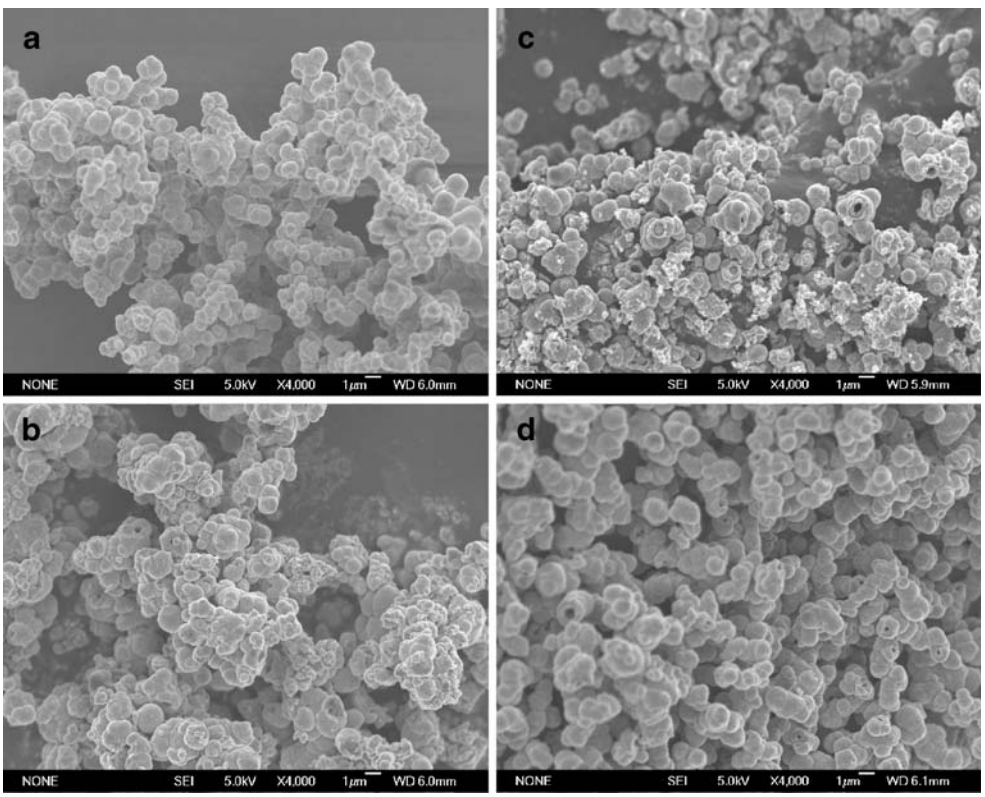

Fig. 5 SEM images of SnO_2 products prepared at 180 °C for **a** 3, **b** 6, **c** 12, and **d** 24 h

The composition of the upper organic phases was identified by the GC–MS analysis. Figure 6 shows the obtained chromatogram with individual peaks analyzed by MS. The largest peak at 1.26 min. corresponds to ethyl chloride, ether, and ethylene glycol diethyl ether. Another modest peak at 5.61 min is attributed to benzyl ethyl ether. The small peaks (marked with an asterisk) are attributed to other condensation products and are not discussed in detail due to their low quantity. Thus, the GC–MS analysis confirms the dehydration reaction of EtOH occurred in our experiment.

On the basis of these observations, the formation of SnO_2 hollow microspheres was proposed as follows: Because of H_2O through the dehydration of EtOH, $SnCl_4$ would initially hydrolyze and condense to produce primary SnO_2 nanocrystals. Subsequently, big solid microspheres would form through the aggregation of these primary SnO_2 nanocrystals. This process was very quick and completed after 3 h, so these renascent solid spheres might not be well crystallized, especially for the nanoparticles inside the solid spheres. Therefore, these inner nanoparticles with higher surface energies would dissolve to form a core–shell structure under the solvothermal conditions, as revealed by Fig. 5c. The dissolved tin ions would further hydrolyze and condense to form SnO_2 nanocrystals on the surface of the spheres. This process was governed by the well-known inside-out Ostwald ripening mechanism. Finally, hollow structured spheres would form after the complete dissolution of the nanoparticles inside the microspheres. This similar inside-out evacuation phenomena was also observed in the formation of other hollow structural materials [21, 24].

The lithium storage behavior of the as-prepared hollow SnO_2 microspheres was tested by means of CV and galvanostatic cycling. Figure 7 shows the CV curves of hollow SnO_2 electrode performed at a scan rate of 0.5 mV s^{-1} in the voltage range of 0.005–2 V vs. Li/Li^+. During the first cathodic scan, a shoulder peak at 0.6 V is observed which can be ascribed to the onset of reduction of SnO_2 to form the Sn metal. This is followed by a smooth sloping curve and a broad peak at 0.1 V. This peak can be attributed to the formation of $Li_{4.4}Sn$ alloy. In the reverse anodic scans, only one well-defined peak at 0.8 V is observed. On the second cycle, the CV curve shows a broad

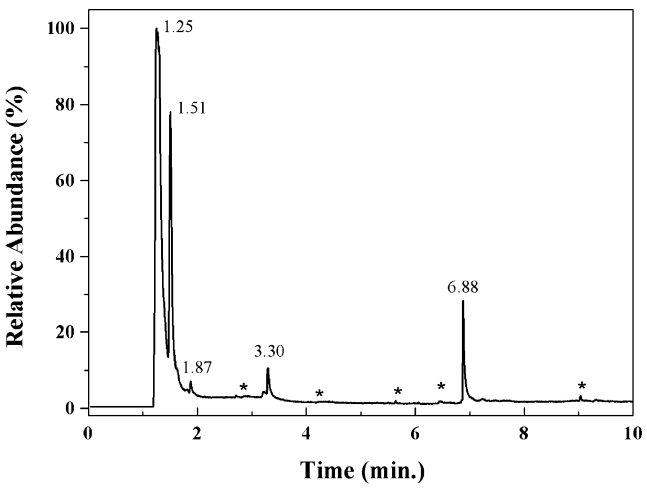

Fig. 6 GC–MS analysis of the organic phase of the postreactive solutions of 18 mL of anhydrous EtOH-condensed H_2SO_4 mixed solvent with 0.6 mL H_2SO_4 at 180 °C for 24 h

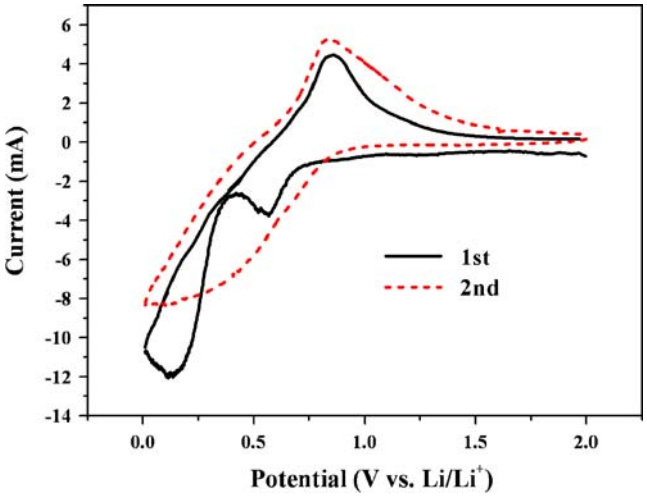

Fig. 7 Cyclic voltammograms of the hollow SnO_2 electrode in the voltage range of 0.005–2.0 V at the scan rate 0.5 mV s^{-1}

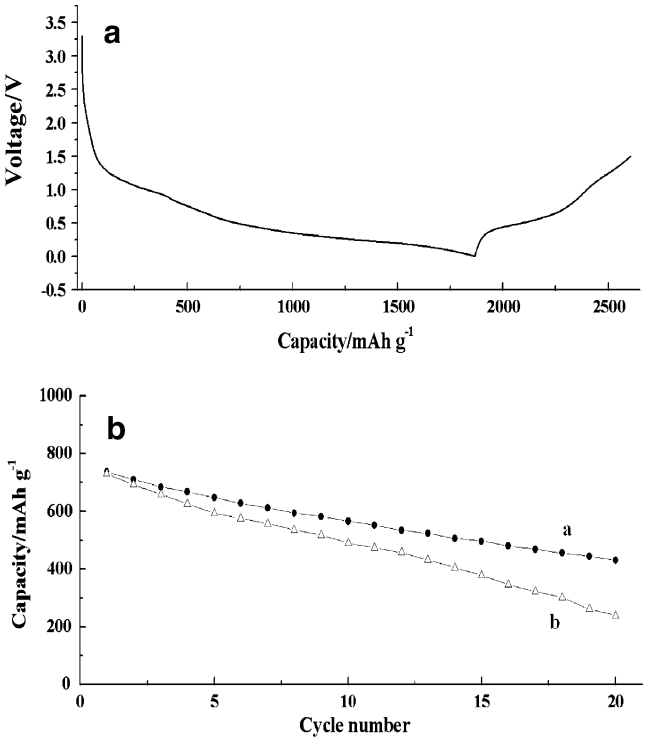

Fig. 8 **a** First charge–discharge profile of hollow SnO_2 microspheres. **b** comparison of cyclability of hollow SnO_2 microspheres with SnO_2 nanoparticles at 100 mA g^{-1} in the voltage window of 0.005–1.5 V

reduction peak at ~0.2 V and intensive oxidation peak at 0.8 V, respectively, for alloying and dealloying reaction [27].

Figure 8a shows the first discharge–charge curve of the SnO_2 electrode at 100 mA g^{-1} in the voltage window of 0.005–1.5 V. The electrode shows a high discharge capacity of 1,867 mAh g^{-1} and charge capacity of 738 mAh g^{-1}, close to its theoretical specific capacity (ca. 790 mAh g^{-1}), indicating the high activity of these hollow spheres due to the large surface area. However, it undergoes great capacity consumption in the first discharge cycle, which can be attributed to irreversible reduction of SnO_2 into elemental Sn and Li_2O and decomposition of the solvent in the electrolyte to form the solid electrolyte interphase. Figure 8b compares the cycling performance of as-prepared SnO_2 hollow nanospheres with pristine SnO_2 nanoparticles obtained via solvothermal reaction at 180 °C for 24 h in 18 mL of anhydrous EtOH in the absence of condensed H_2SO_4. While the capacities of both materials decreased with the cycle numbers, the hollow SnO_2 microspheres apparently exhibited a better cycle performance than that of SnO_2 nanoparticles. This enhanced cyclability has also been observed in other hollow SnO_2 electrodes [4, 8, 11, 14]. It is known that the poor cyclability of bulk SnO_2 is due to the large volume change (about 358%) during charge–discharge process, which leads to mechanical failure and the loss of electrical contact. Although reducing the SnO_2 particles to nanodimensions can render the phase transitions that accompany alloy formation more facile and reduces cracking within the electrode, nano-SnO_2 does not sufficiently reduce the extent of volume change. The hollow structure instead would be able to offer free space to accommodate the volume expansion during lithium uptake [28]. Moreover, it is suggested that the hollow structure can recapture the SnO_2 nanoparticles once they are detached from the internal surface [8]. Thus, hollow SnO_2 can cycle lithium better than nano-SnO_2.

Conclusion

In summary, we have demonstrated a one-pot synthesis of the hollow SnO_2 microspheres. The reaction process consists of the controlled hydrolysis and condensation of $SnCl_4$ by the formation of water via catalytic dehydration of EtOH in the presence of condensed H_2SO_4 and the subsequent inside-out Ostwald ripening process. This current method is simple and template-free and provides an alternative approach to prepare transition metal oxide hollow spheres. The as-prepared hollow SnO_2 microspheres exhibited better cycle performance than the pristine SnO_2 nanoparticles when used as anode materials in lithium ion batteries.

Acknowledgments This work was supported by National Basic Research Program of China (973 Program) (Grant 2007CB613301), National Science Foundation of China (Grants 20503009, and 20777026), Program for New Century Excellent Talents in University (Grant NCET-07-0352), the Key Project of Ministry of Education of China (Grant 108097), and the Scientific Research Foundation for the Returned Overseas Chinese Scholars, State Education Ministry.

References

1. Vayssieres L, Graetzel M (2004) Angew Chem Int Ed 43:3666
2. Duan JH, Yang SG, Liu HW, Gong JF, Huang HB, Zhao XN, Zhang R, Du YW (2005) J Am Chem Soc 127:6180
3. Wang Y, Zeng HC, Lee JY (2006) Adv Mater 18:645
4. Lou XW, Wang Y, Yuan CL, Lee JY, Archer LA (2006) Adv Mater 18:2325
5. Yu JG, Guo HT, Davis SA, Mann S (2006) Adv Funct Mater 16:2035
6. Yang HX, Qian JF, Chen ZX, Ai XP, Cao YL (2007) J Phys Chem C 111:14067
7. Qian JF, Liu P, Xiao Y, Jiang Y, Cao YL, Ai XP, Yang HX (2009) Adv Mater. doi:10.1002/adma.200900525
8. Wang Y, Su F, Lee JY, Zhao XS (2006) Chem Mater 18:1347
9. Han S, Jang B, Kim T, Oh SM, Hyeon T (2005) Adv Funct Mater 15:1845
10. Ba JH, Polleux J, Antonietti M, Niederberger M (2005) Adv Mater 17:2509
11. Li M, Lu Q, Nuli Y, Qian X (2007) Electrochem Solid-State Lett 10:K33
12. Sun X, Liu J, Li Y (2006) Chem Eur J 12:2039
13. Xu H, Wang W (2007) Angew Chem Int Ed 46:1489
14. Deng D, Lee JY (2008) Chem Mater 20:1841
15. Titirici MM, Antonietti M, Thomas A (2006) Chem Mater 18:3808
16. Fan HJ, Knez M, Scholz R, Nielsch K, Pippel E, Hesse D, Zacharias M, Goesele U (2006) Nat Matters 5:627
17. Gao JH, Liang G, Zhang B, Kuang Y, Zhang XX, Xu B (2007) J Am Chem Soc 129:1428
18. Peng Q, Dong Y, Li Y (2003) Angew Chem Int Ed 42:3027
19. Yang HG, Zeng HC (2004) J Phys Chem B 108:3492
20. Wang WS, Zhen L, Xu CY, Zhang BY, Shao WZ (2006) J Phys Chem B 110:23154
21. Li J, Zeng HC (2007) J Am Chem Soc 129:15839
22. Wang Y, Zhu Q, Zhang H (2005) Chem Commun 41:5231
23. Cao X, Gu L, Zhuge L, Gao W, Wang W, Wu S (2006) Adv Funct Mater 16:896
24. Li B, Rong G, Xie Y, Huang L, Feng C (2006) Inorg Chem 45:6404
25. Fan J, Wang T, Yu C, Tu B, Jiang Z, Zhao D (2004) Adv Mater 16:1432
26. Qiao H, Zheng Z, Zhang L, Xiao L (2008) J Mater Sci 43:2778
27. Ahn HJ, Choi HC, Park KW, Kim SB, Sung YE (2004) J Phys Chem B 108:9815
28. Bruce PG, Scrosati B, Tarascon JM (2008) Angew Chem Int Ed 47:2930